Investigation of crystallization process in isotropic rare-earth-rich (Nd or Pr)–Fe–B films

Cite as: AIP Advances **13**, 025006 (2023); https://doi.org/10.1063/9.0000617
Submitted: 12 October 2022 • Accepted: 17 November 2022 • Published Online: 03 February 2023

I. Fukuda, K. Higashi, K. Higuchi, et al.

Investigation of crystallization process in isotropic rare-earth-rich (Nd or Pr)–Fe–B films

Cite as: AIP Advances 13, 025006 (2023); doi: 10.1063/9.0000617
Submitted: 12 October 2022 • Accepted: 17 November 2022 •
Published Online: 3 February 2023

I. Fukuda, K. Higashi, K. Higuchi, A. Yamashita, T. Yanai, H. Fukunaga, and M. Nakano[a]

AFFILIATIONS

Graduate School of Engineering, Nagasaki University, Nagasaki 852-8521, Japan

Note: This paper was presented at the 67th Annual Conference on Magnetism and Magnetic Materials.
[a]**Author to whom correspondence should be addressed:** mnakano@nagasaki-u.ac.jp

ABSTRACT

In this paper, the relationship between the initial crystalline behavior and annealing conditions in pulsed laser deposition (PLD)-made Nd-Fe-B and Pr-Fe-B films with rare-earth-rich composition is discussed. The films with rare-earth-rich compositions are prepared via PLD. An annealing process is necessary to obtain the crystalline 2-14-1 phase of hard magnetic properties because all the as-deposited films have an amorphous structure. In conventional annealing, the initial crystallization of the $Pr_2Fe_{14}B$ phase occurred at lower temperatures compared with that of the $Nd_2Fe_{14}B$ phase, indicating that the annealing temperature of the initial crystallization of the $Pr_2Fe_{14}B$ phase was lower than that of the $Nd_2Fe_{14}B$ phase. Considering the same crystallization temperature in both the phases, the melting points of both rare-earth elements, Nd and Pr, are considered to relate to the initial crystallization behavior. We also confirmed that the annealing time for $Pr_2Fe_{14}B$ phase formation was shorter than that for $Nd_2Fe_{14}B$ phase formation.

I. INTRODUCTION

Many studies have demonstrated small electronic devices including (Nd or Pr)–Fe–B thick-film magnets prepared via sputtering[1–3] and pulsed laser deposition (PLD),[4–6] whereas aerosol deposition[7] and 3D printing[8] constitute the room-temperature processes for preparing small rare-earth magnets. Both sputtering and pulsed laser deposition require an annealing process such as substrate heating and/or post annealing. Reducing the annealing temperature and/or time can result in wider applications of the films because a flexible material with low softening point can be used in application devices. However, it is difficult to decrease the annealing temperature and/or time drastically for PLD-made films. Therefore, we focus on fundamental experiments such as crystallization of PLD-made (Nd or Pr)–Fe–B films under various annealing conditions in the present study, and we compare the initial crystallization behavior in isotropic Nd–Fe–B and Pr–Fe–B films with rare-earth-rich composition.

II. EXPERIMENTAL PROCEDURE

A rotated (Nd or Pr)–Fe–B target was ablated using a neodymium-doped yttrium aluminum garnet (Nd: YAG) pulse laser (wavelength = 355 nm, repetition frequency = 30 Hz) under vacuum conditions of approximately 10^{-5} Pa. A (Nd or Pr)–Fe–B film was deposited using a defocus rate of 0.3.[9] To crystallize the as-deposited (Nd or Pr)–Fe–B films, which have an amorphous structure, the following two methods were used. (1) Conventional annealing by a resistance heating furnace (heating rate 225–350 °C/min, temperature: 450–700 °C, holding time: 0 s) and (2) pulse(flash)–annealing[10] using an infrared furnace with time ranging from 1.6 to 2.4 s. The conditions of the conventional annealing are almost the same as those reported in the Ref. 6.

The magnetic properties of the annealed samples were measured after magnetizing each sample with a pulsed magnetic field of 7 T using a vibrating sample magnetometer under a maximum applied magnetic field of 2.5 T. Because all films exhibited isotropic magnetic properties, only in-plane ones are discussed here. The thickness of each film was measured using a micrometer. The compositions of the (Nd or Pr)–Fe–B films were analyzed using energy-dispersive X-ray spectroscopy.

III. RESULT AND DISCUSSION

A. Coercivity and crystallization behavior as a function of annealing temperature in conventional annealing

In this section, coercivity and crystalline structure of (Nd or Pr)–Fe–B films annealed at various temperatures are discussed. The

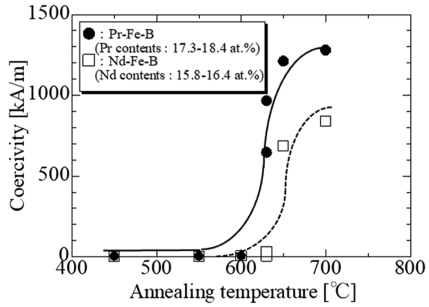

FIG. 1. Coercivities of Pr–Fe–B and Nd–Fe–B films as a function of annealing temperature in conventional annealing. The coercivity enhanced with the temperature. In particular, the coercivities of both the films were significantly different at 630 °C.

rare-earth contents of Nd–Fe–B and Pr–Fe–B films used here are 15.8–16.4 at.% and 17.3–18.4 at.%, respectively. Figure 1 shows the average coercivity of magnet films as a function of the annealing temperature using a resistance heating furnace. The coercivity values of both the films are ultimately low at the annealing temperature of 450 °C–600 °C. In addition, the Nd–Fe–B films annealed at 630 °C exhibit low coercivity. In contrast, the coercivity of Pr–Fe–B films exceeds 500 kA/m at 630 °C. We consider that the magnetic

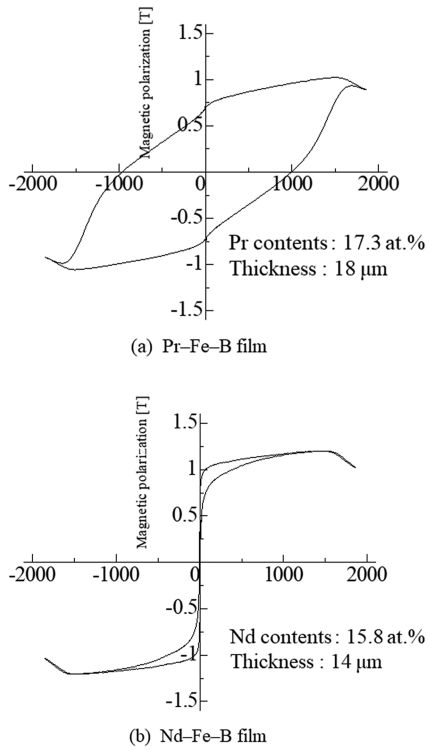

FIG. 2. J-H loops of Pr–Fe–B and Nd–Fe–B films annealed at 630 °C in conventional annealing. The Pr–Fe–B film had large coercivity. In contrast, the Nd–Fe–B film did not exhibit hard magnetic properties due to the existence of the soft magnetic phase.

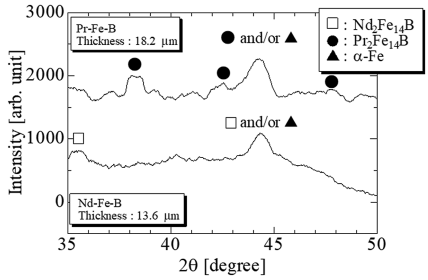

FIG. 3. Crystalline structure of Pr–Fe–B and Nd–Fe–B films annealed at 630 °C in conventional annealing. The 2–14–1 phase formation of the Pr–Fe–B film progresses faster compared with that of the Nd–Fe–B film.

hysteresis loop in Fig. 2(a) shows a staircase-like profile which suggests the coexistence of two magnetic phases of $Pr_2Fe_{14}B$ and α-Fe phase because the knick of the loop shows around the remanence. The shapes of J-H loops are significantly different in both films annealed at 630 °C (Fig. 2). As shown in Fig. 3, the progress of 2-14-1 phase formation in the Pr–Fe–B film is faster than that in the Nd–Fe–B film. Considering the same crystallization temperature of $Nd_2Fe_{14}B$ and $Pr_2Fe_{14}B$,[11] the phenomenon is considered to relate to the different melting points of Pr (930 °C) and Nd (1024 °C). However, further investigation of the mechanism is required. At 650 °C and 700 °C, the coercivity values of the Pr–Fe–B films are larger than those of the Nd–Fe–B films, which can be attributed to the higher magnetic crystalline anisotropy constant of the $Pr_2Fe_{14}B$ phase (Ku = 6.8 MJ/m^3) by approximately 2.3 MJ/m^3 than that of the $Nd_2Fe_{14}B$ phase (Ku = 4.5 MJ/m^3).

These results indicate that the initial crystallization behavior as a function of annealing temperature is different between isotropic Pr–Fe–B and Nd–Fe–B films with a rare-earth-rich composition.

B. Coercivity and crystallization behavior as a function of rime in the pulse-annealing

To form the 2–14–1 phase, we mainly used pulse–annealing[10] instead of conventional annealing for the as-deposited (Nd or Pr)–Fe–B amorphous structure prepared via PLD because pulse–annealing is effective in reducing grain size and suppressing oxidation. Figure 4 shows coercivity as a function of annealing time. The rare-earth contents of the Pr–Fe–B and Nd–Fe–B

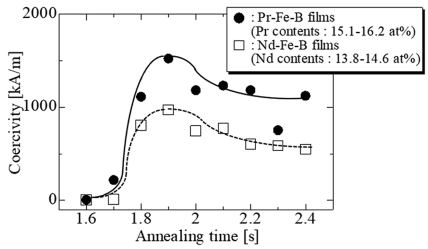

FIG. 4. Coercivity of Pr–Fe–B and Nd–Fe–B films as a function of annealing time in pulse annealing. The coercivity value enhanced with time. At the annealing time of 1.7 s, the average coercivity of Pr–Fe–B films exceeded 200 kA/m. In contrast, the average coercivity of Nd–Fe–B films was ultimately low.

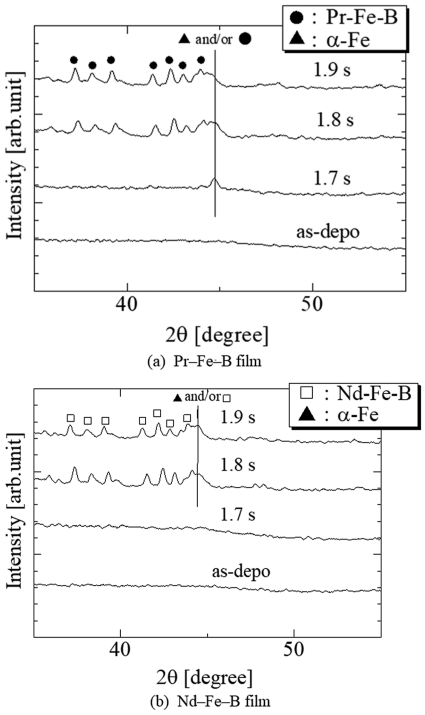

FIG. 5. Crystalline structure of Pr–Fe–B and Nd–Fe–B films as a function of annealing temperature in pulse annealing. The 2-14-1 phase formation of the Pr–Fe–B film occurred at 1.7. In contrast, the Nd–Fe–B film did not show an X-ray diffraction peak (amorphous structure).

films used here were 15.1–16.2 at. % and 13.8–14.6 at. %, respectively. The thickness range of both magnet films is between 10 and 31 μm. Here, the coercivity at each annealing time is an average value of several samples. The coercivity is significantly low at an annealing time of 1.6–1.7 s. At the annealing time of 1.8 s, the coercivity significantly increases in both the films. In particular, we focus on the slight difference of coercivity at 1.7 s. As shown in Fig. 5, the 2-14-1 phase formation of the Pr–Fe–B film starts at 1.7 s, whereas the Nd–Fe–B film has an amorphous structure. These results suggest the similar tendency of initial crystallization behavior between isotropic Pr–Fe–B and Nd–Fe–B films with rare-earth-rich composition.

IV. CONCLUSIONS

In the study, the relationship between crystalline process and annealing conditions of PLD-made Nd–Fe–B and Pr–Fe–B thick-films with rare-earth-rich contents was compared. In the conventional annealing method, the initial crystallization of the $Pr_2Fe_{14}B$ phase occurred at lower temperatures compared with that of the $Nd_2Fe_{14}B$ phase. This result indicates that the annealing temperature of the initial crystallization of $Pr_2Fe_{14}B$ phase was lower than that of the $Nd_2Fe_{14}B$ phase. Considering the same crystallization temperature in both the phases, each melting point of the rare-earth elements of Nd and Pr is considered to relate to the initial crystallization behavior. We also confirmed that the annealing time of the formation of $Pr_2Fe_{14}B$ phase was shorter than that of $Nd_2Fe_{14}B$ phase. Based on the findings of this fundamental study, we will advance the low temperature process of PLD-made films as future work.

ACKNOWLEDGMENTS

This work was supported by JSPS KAKENHI under Grant JP 19H02173 and 19H00738 and by Nagasaki University State of the Art Research program.

AUTHOR DECLARATIONS

Conflict of Interest

The authors have no conflicts to disclose.

Author Contributions

I. Fukuda: Investigation (equal). **K. Higashi**: Investigation (supporting). **K. Higuchi**: Investigation (lead). **A. Yamashita**: Investigation (supporting). **T. Yanai**: Investigation (supporting). **H. Fukunaga**: Investigation (supporting). **M. Nakano**: Supervision (equal).

DATA AVAILABILITY

The data that support the findings of this study are available from the corresponding author upon reasonable request.

REFERENCES

[1] R. Fujiwara, T. Shinshi, and M. Uehara, Int. J. Autom. Technol. **7**, 148 (2013).
[2] R. Fujiwara, T. Shinshi, and E. Kazawa, Sens. Actuators, A **220**, 298 (2014).
[3] S. Yamashita, J. Yamasaki, M. Ikeda, and N. Iwabuchi, J. Magn. Soc. Jpn. **15**, 241 (1991).
[4] M. Nakano, S. Takeichi, T. Yamaguchi, K. Takashima, A. Yamashita, T. Yanai, T. Shinshi, and H. Fukunaga, Jpn. J. Appl. Phys. **59**, SEEE01 (2019).
[5] M. Nakano, T. Honda, J. Yamasaki, S. Sato, F. Yamashita, J. Fidler, and H. Fukunaga, Sens. Lett. **5**, 48 (2007).
[6] M. Nakano, S. Sato, F. Yamashita, T. Honda, J. Yamasaki, K. Ishiyama, M. Itakura, J. Fidler, T. Yanai, and H. Fukunaga, IEEE Trans. Magn. **43**, 2672 (2007).
[7] S. Sugimoto, T. Maki, T. Kagotani, J. Akedo, and K. Inomata, JMMM **290–291**, 1202 (2005).
[8] Z. Wang, C. Huber, J. Hu, J. He, D. Suess, and S. X. Wang, Appl. Phys. Lett. **114**, 013902 (2019).
[9] H. Fukunaga, T. Kamikawatoko, M. Nakano, T. Yanai, and F. Yamashita, J. Appl. Phys. **109**, 07A758 (2011).
[10] H. Fukunaga, K. Tokunaga, and J. M. Song, IEEE Trans. Magn. **38**, 2970 (2002).
[11] T. Nguyen Van, I. de Moraes, N. M. Dempsey, C. Champeaux, and F. Dumas-Bouchiat, JMMM **520**, 167584 (2021).